Electronic Supplementary Material (ESI) for Nanoscale.
This journal is © The Royal Society of Chemistry 2019

Supplementary Information

Title

Tunable electronic properties by ligand coverage control in PbS nanocrystal assemblies

Authors

Liming Liu,[a] Satria Zulkarnaen Bisri,[b*] Yasuhiro Ishida,[b*] Takuzo Aida,[a,b] and Yoshihiro Iwasa[b,c]

Affiliations

[a] Department of Chemistry and Biotechnology, School of Engineering, The University of Tokyo, 7-3-1 Hongo, Bunkyo-ku, Tokyo 113-8656, Japan.

[b] RIKEN Center for Emergent Matter Science, 2-1 Hirosawa, Wako, Saitama 351-0198, Japan.

[c] Quantum-Phase Electronics Center and Department of Applied Physics, The University of Tokyo, 7-3-1 Hongo, Bunkyo-ku, Tokyo 113-8656, Japan.

Corresponding Author Email: satria.bisri@riken.jp; y-ishida@riken.jp

A. PbS Colloidal Quantum Dots and Assemblies Morphology

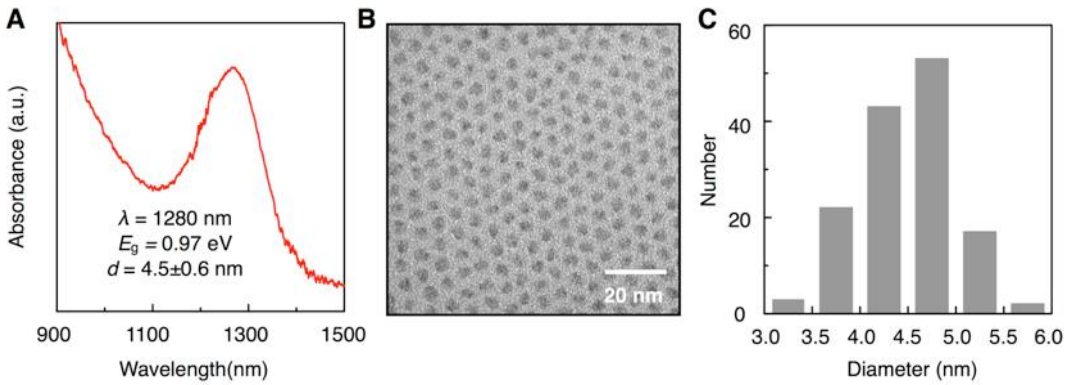

Fig. S1. Characterization of the native PbS NCs (capped with oleic acid). (A) The absorption spectrum in chloroform. (B) TEM image. (C) Histogram of the diameter.

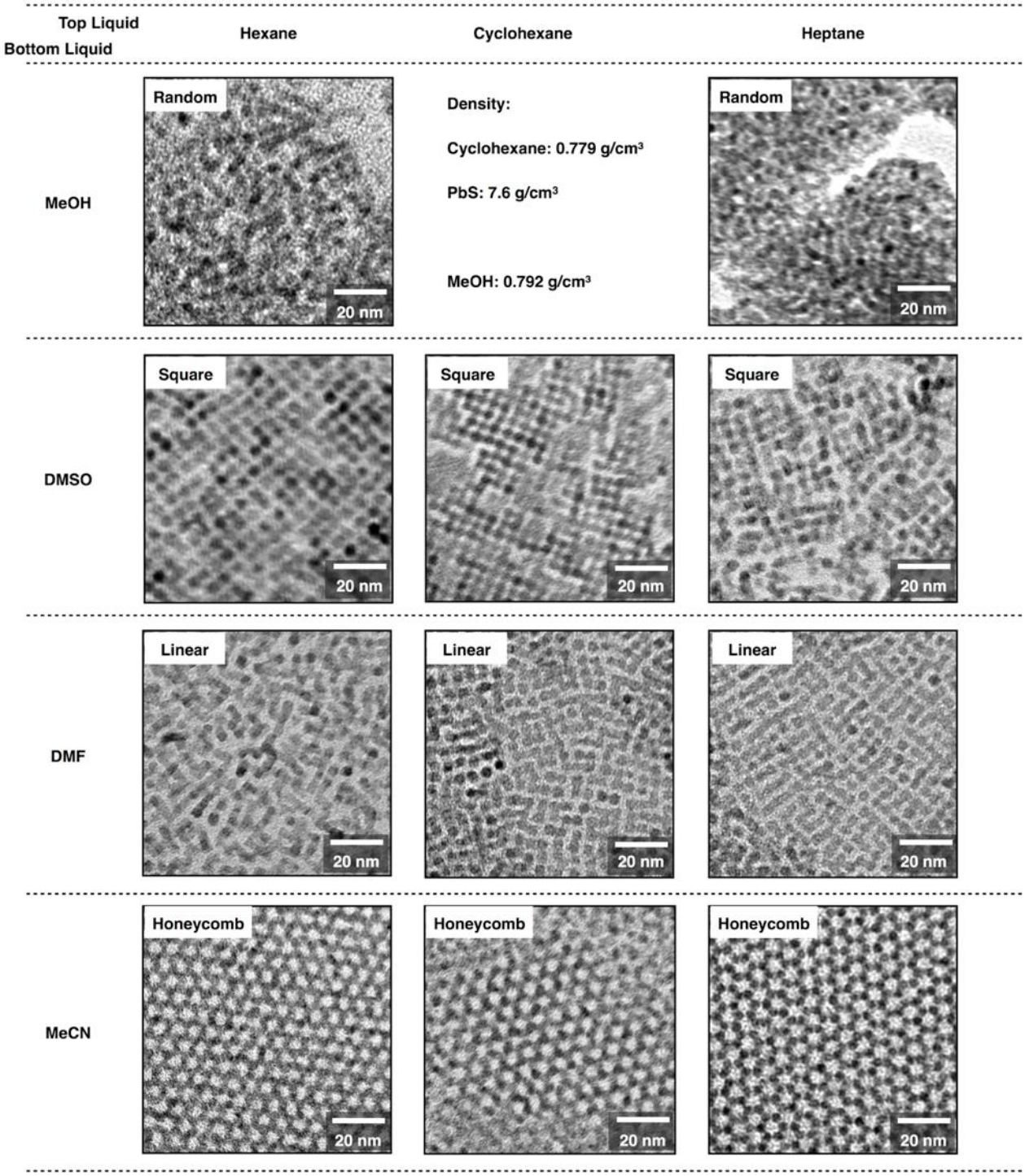

Fig. S2. Transmission electron micrograph (TEM) images of liquid/air assemblies of PbS NCs with various combinations of the bottom and top liquids. Due to the density problem, this method cannot work for the combination of cyclohexane as the top liquid and MeOH as the bottom liquid. The bottom liquids have a significant influence on assembly structures. However, top liquids have little effect on the assembly patterns.

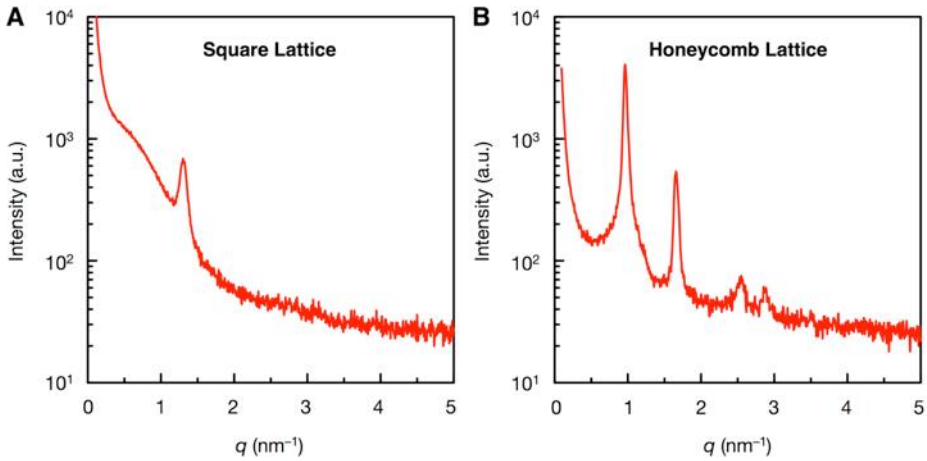

Fig. S3. 1D profiles deduced from the 2D images of GISAXS, which are used to calculate the inter-NCs distance of: (**A**) DMSO-generated square lattice. (**B**) MeCN-generated quasi-honeycomb lattice.

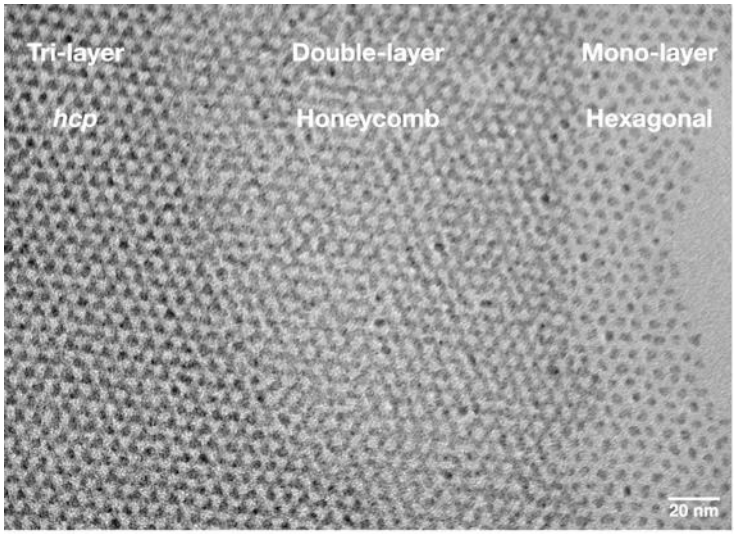

Fig. S4. The TEM image of a PbS NC film prepared by the usage of MeCN as the bottom liquid. The film shows domains with various numbers of layers: (right side) Mono-layer of PbS NCs forming hexagonal lattice; (central) double-layer of PbS NCs showing quasi-honeycomb lattice; (left side) tri-layer of PbS NCs showing the hcp (hexagonal closed pack) lattice.

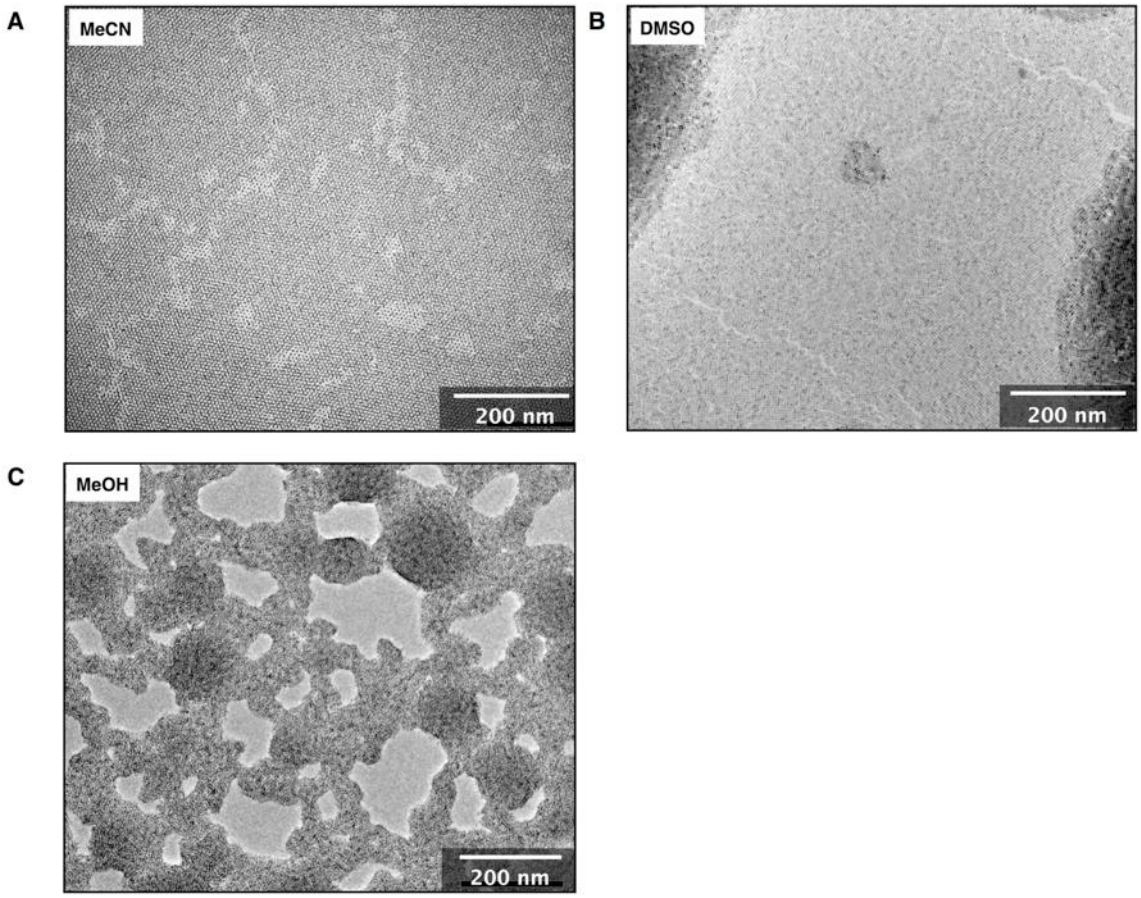

Fig. S5. TEM images of different PbS NC films prepared by the use of various bottom liquids: (**A**) MeCN, (**B**) DMSO, and (**C**) MeOH.

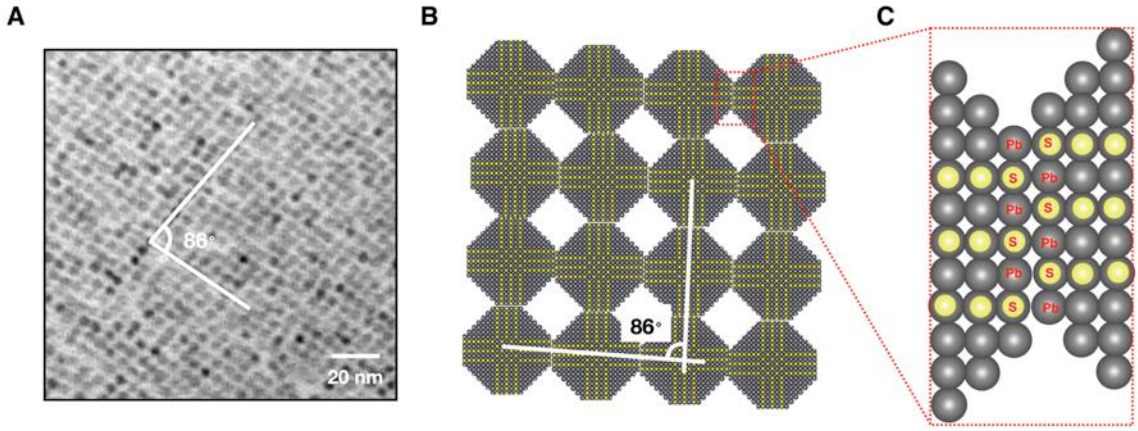

Fig. S6. Square lattice made by DMSO with a lattice angle of 86°. (**A**) The TEM image of the PbS NC square lattice formed by the use of DMSO as the bottom liquid, exhibiting a lattice angle of 86°. (**B**) Illustration of the lattice of PbS NCs connected with an angle of 86°. As a PbS NC has its own crystal structure, the off-set of NCs connection is created due to the Pb-S-Pb-S bonding. (**C**) Magnified illustration showing the bonding area of neighboring PbS NCs.

B. Ligand Density

(1) *Ligand Density of original PbS NCs*

The ligand density of the original PbS NCs (after 3 times' washing) is determined by thermo gravimetric analysis (TGA). From a calculated surface area of 175 m^2 g^{-1} (based on a 4.5 nm diameter and 7.6 g cm^{-3} bulk density) and a TGA mass loss of 20% around 380 °C (Fig. S9), a surface coverage of 3.0 ligand/nm^2 can be approximated, which is consistent with the literature. [1]

(2) *Ligand Density of PbS NC films treated by different bottom liquids*

The ligand density of PbS NC films treated by different bottom liquids is indirectly determined by ^{1}H NMR. As it is very hard to directly determine the ligand density of solid PbS NC samples, the oleic acid amount on the NC films is indirectly calculated by the dissolved oleic acid in the bottom liquids, where dissolved oleic acid amounts into different bottom liquids (MeCN, DMSO, MeOH) can be quantified by ^{1}H NMR. From the oleic acid removal percentage of each bottom liquid and original oleic acid coverage 3.0 ligand/nm^2, the ligand density of different bottom liquid treated PbS NC films can be determined. The detailed calculation is shown in Table S1.

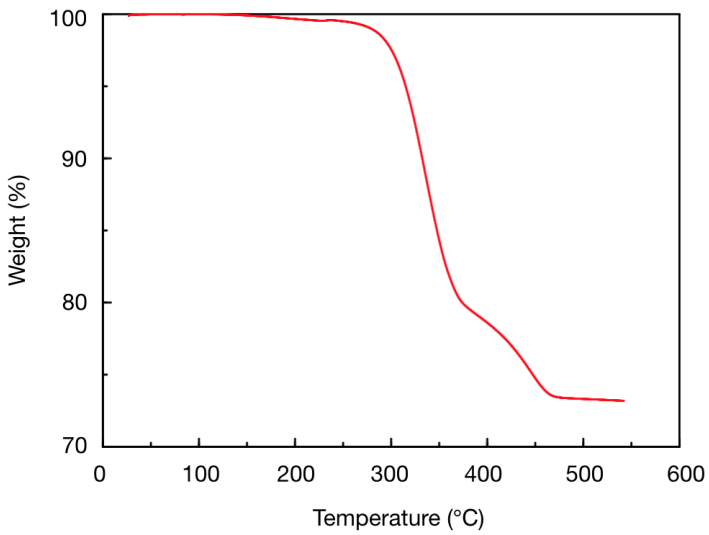

Fig. S7 Thermo gravimetric analysis (TGA) of the original PbS NCs (after 3 times' washing). The mass loss up to 380 °C is from the burning of oleic acid. The mass loss from 380 °C to 460 °C is regarded to unknown purities, which is also shown in other PbS NC as well. [1]

Table S1 Ligand density of PbS NC films treated by different bottom liquids

	Area of ^{1}H NMR peak	Amount of oleic acid determined by NMR (μmol)	Oleic acid removal percentage (%)	Oleic acid density on PbS NC surface (ligand/nm^2)
MeCN	0.19	0.048	21.46%	2.4
DMSO	0.30	0.069	30.89%	2.1
MeOH	0.83	0.171	76.30%	0.7

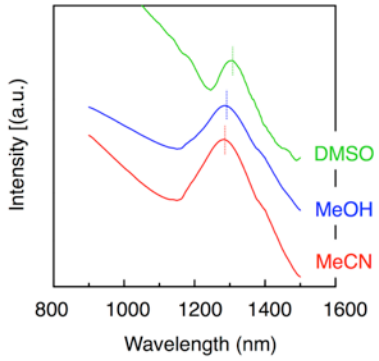

Fig. S8. UV/Vis/NIR absorption spectra of the PbS NC films prepared by the use of various bottom liquids: DMSO (green), MeOH (blue) and MeCN (red). The PbS NC films fabricated by MeOH and MeCN show similar absorption peak with PbS NCs in solution form, which means that the PbS NCs in the MeOH and MeCN made NC films are separated with each other. It is straightforward to understand that MeCN made NC films are the NCs separated with oleic acid. However, it is difficult to recognize that MeOH made NC films still give the separated NCs, instead of attached NCs, although the oleic acid on the surface of NCs is almost completely removed by MeOH. For these reasons, we infer that MeOH removes the oleic acid so fast that there is no time for NCs to orientate their facets for attachments. As facets on NCs cannot attach with each other, NCs in the MeOH made films only show aggregation of separated NCs, which show similar absorption spectrum with MeCN made films.

C. Mobility Calculation in EDLTs

To extract the values of the charge carrier mobilities in the EDLTs, we need to estimate the accumulated carrier density in the PbS NC channel. In solid SiO_2-gated FET, the dielectric capacitance is relatively constant for almost the whole gate voltage scan, and its value is only determined by the dielectric constant and layer thickness. On the other hand, the capacitance of the EDL gate varies and tends to increase by the applied gate voltage. This variation arises from the more compact accumulations of ions at the electric double layer by higher traverse electric field (higher effective V_G) and the influence of how the density of states of the measured semiconductor channel.

For the carrier density estimation in this paper, we performed the gate displacement current measurement. [2,3] The low conductivity of the system prevents us from performing evaluation by Hall effect measurements, and the small size of the device made difficulty in performing electrochemical impedance spectroscopy at low frequencies on the identical transistor with minimum noise. We extracted the gate-dependent carrier density via the integration of gate displacement current as a function of time [4]. From the same EDLT device, we obtained the displacement current (I_{Disp}) from the gate current (I_G) measurement, while shorting and grounding the source and drain electrodes, to form an EDL capacitor circuit. In the forward sweep, the measured current corresponds to the process occurred during the capacitor charging, while the reverse sweep corresponds to its discharge. This I_G (V_G) is composed of the sum of: (i) electronic leakage at both interfaces of the ionic liquid capacitor; and, (ii) ionic displacement current (I_{Disp}), by which the charges at the semiconductor side are accumulated. The former is reflected by the trend of I_G prior to the turn-on of the device (before the threshold of I_D enhancement). [3]

The total accumulated electron density in the transistor channel can be estimated from the integration of the displacement current:

$$n = \frac{Q}{eA} = \frac{\int I_{Disp} dV_G}{eA(dV_G/dt)} \tag{1}$$

where A is the charge carrier accumulated area, I_{Disp} is the displacement current (the shaded area of Figure S9b and S10b), and dV_G/dt is the sweep rate of the applied gate voltage. Here the sweep rate is associated with the value used for I_D–V_G transfer characteristic measurement. The lower integration limit of the I_{Disp} is from the threshold of the electron current enhancement. The gate-dependent electron carrier density is plotted in Figure S9c and S10c.

From both the gate-dependent I_D and gate-dependent n, we can extract the electron mobility through the following relation.

$$\mu = \frac{L}{W} \cdot \frac{1}{eV_D} \cdot \frac{I_D}{n} \tag{2}$$

Thus, the gate-dependent mobility can be plotted as Figure S9d and S10d, with the maximum mobility value reaching 1.5 $cm^2\ V^{-1}\ s^{-1}$ for the [DEME][TFSI]-gated device.

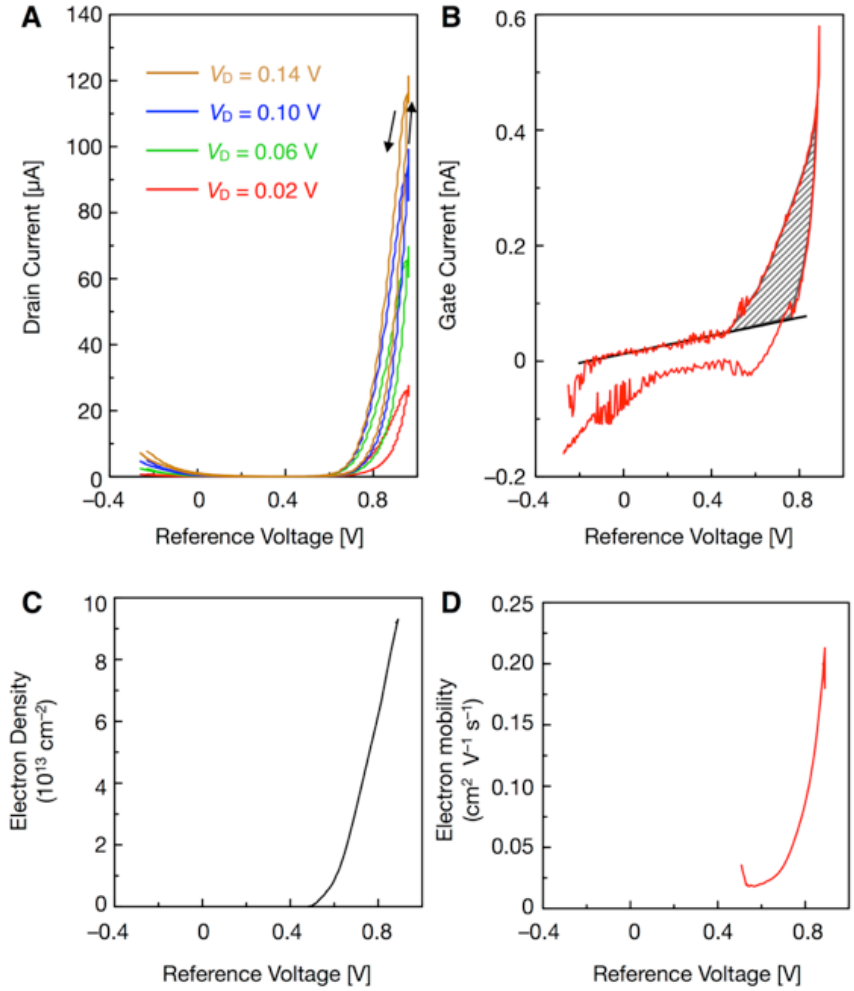

Fig. S9. Mobility extraction based on carrier density estimated by the displacement current of the [EMIM][TFSI] ionic liquid gating. (**A**) I_D–$V_{G.REF}$ transfer characteristic of the square lattice of PbS NCs. (**B**) I_G–$V_{G.REF}$ curve of the same device, operating as EDL capacitor. The shaded area is the displacement current area where the integration yields the accumulated carrier density by the electric double layer gating. (**C**) Electron density as a function of the reference gate voltage estimated by Equation (1). (**D**) Gate-dependent electron mobility corresponding to (A)–(C).

Table S2 Variations of Extracted Electron Mobility

Device No.	Electron Mobility* ($cm^2 V^{-1} s^{-1}$)
1	0.288
2	0.067
3	0.449
4	0.182
5	0.112
6	0.274
7	0.217
Average	0.227
Std. error	0.127

*) the maximum value of the gate-dependent mobility

D. Discussion of mobility value in PbS square lattice

Compared with record mobility value of PbX (X=S, Se, Te) NCs, the mobility value of the PbS square lattice 0.23 ± 0.13 $cm^2 V^{-1} s^{-1}$ in this work is much lower.
There are several reasons for this low mobility values:

First of all, it should be noted that the extracted value of carrier mobility in NC transistors is affected not only by the assembly structure of the NCs in the transistor channel but also by many other parameters. Some of the parameters are channel-material related (in this case: NC compound, usage of ligands, doping or trap condition of the NC), while some others are device-related (FET structures, gating condition: type of gating that is being used). Most of the reported atomically connected lattices are also on PbSe NC assemblies.[5] Charge carrier transport in NC assemblies can be affected by the bulk nature of the constituent NC as well as by the inter-particle charge transport, governed by the electronic coupling. Intrinsically in their bulk form, PbSe has larger electron mobility values than PbS. Furthermore, the exciton Bohr radius of PbSe is much larger than PbS; thus, the electronic coupling between PbSe NCs is much stronger than between PbS NCs at a similar distance. These two factors make the mobility values in PbSe NC assemblies tend to be much larger than PbS NC assemblies, when other factors are excluded. Therefore, it is acceptable that the mobility values obtained from our PbS NC assemblies are lower than many other reports, which used PbSe NCs by about one order of magnitude.

Secondly, it should be noted that the high dielectric coefficient of Pb-chalcogenide NCs (ε_{PbS} ~22) makes the transistor to have a thick accumulation/depletion layer. As consequences, there are variations of the deduced charge carrier mobility values proportional to the thickness of NC assemblies.[6] In most of the reported literature, the thickness of the NC assemblies was at least several monolayers, if not thicker. In our current manuscript, the NC assemblies used in the transistor channel are mainly a single monolayer.

To the best of our knowledge, for transistors with undoped PbS NC system, the best typical electron mobility values were around 10^{-2} $cm^2 V^{-1} s^{-1}$ using solid oxide gate devices. The usage of halide ligands also provides electron mobility values around that order. It was the use of hydroxyl-

free polymer gates that demonstrate electron mobility values in the order of 10^{-1} cm^2 V^{-1} s^{-1}.[7] The use of ionic liquid gating or high-k block copolymer capable of accumulating very high carrier density, thus filling the electron trap sites, were able to demonstrate electron mobility values in PbS NC assemblies up to 1 cm^2 V^{-1} s^{-1} (Table S3).[8] Again, this should be noted that the demonstration of the abovementioned electron mobility values was deduced from devices with several monolayers of NC assemblies.

In this manuscript, we present the electron mobility values from three different types of PbS NC assemblies. The values were extracted from devices containing only a monolayer of NC assemblies and from electric-double-layer transistor characteristics, where high carrier density accumulation occurs. We show that through structural improvement via control of ligand coverage and oriented attachment, the electron mobility is enhanced. If later on, we can enlarge further the ordered domain and stack several monolayers of such perfect mesoscopic structure, it is promising to demonstrate much higher electron mobility values.

Table S3 Overview of different treatments and the effect on mobilities in PbX NC FETs.

PbX NC	NC size [nm]	Ligand	Structure	Dielectric	Electron Mobility [cm^{-2} V^{-1} s^{-1}]	Hole Mobility [cm^{-2} V^{-1} s^{-1}]	Ref
PbS	7.1	I^-	Ordered	SiO_2		0.2	[9]
PbS	11	SCN^-	Ordered	Parylene	0.1	0.1	[10]
PbS	4.5	No ligand	Ordered	Electrolyte	0.23		This work
PbSe	5.8	No ligand	Ordered	SiO_2	0.5		[5]
PbSe	5.5	No ligand	Ordered	Electrolyte	5-18		[11]
PbS	3.6	EDT	Random	Electrolyte	1.91	0.15	[6]
PbS	3.15	EDT	Random	P(VDF-TrFE-CFE)	1.1		[8]
PbS	3.6	3MPA	Random	Cytop	0.2		[7]
PbSe	8.0	Hydrazine	Random	SiO_2	0.7	0.18	[12]
PbSe	5.0	I^-	Random	SiO_2	0.31		[13]
PbSe	6.3	S^{2-}, Al_2O_3 deposition	Random	SiO_2	7		[14]

E. Discussion on inhomogeneity of ligand stripping

In this work, all the ligand density numbers are calculated in an average manner regardless of inhomogeneity of thickness of NC films and top and bottom difference. However, we want to give some discussion of the inhomogeneity of ligand stripping on NC film formation.

(1) For the inhomogeneity of multi-layer NC films, in principle, the top nanocrystals can not touch with the solvent surface, which could not strip ligands on NC surface to form square lattice. However, from the TEM images (Fig. S10), we found that even multi-layer of NCs still show the formation of square lattice, not hexagonal lattice, which means that the top nanocrystals are definitely affected by the bottom nanocrystals for the structure formation.

(2) For the inhomogeneity of monolayer NC films, there could be some more remaining oleic acid on the top surface of nanocrystals than the bottom surface of the nanocrystals in the assembly films. To prove this experimentally is still very challenging. However, judging from the observation of the square lattice formation in the multi-layer films, efficient selective ligand stripping still occurs at least until the third monolayer. Furthermore, the transport measurement results presented in this

work shows the possible inhomogeneity of the ligand stripping in the vertical direction does not affect so much the planar charge carrier transport.

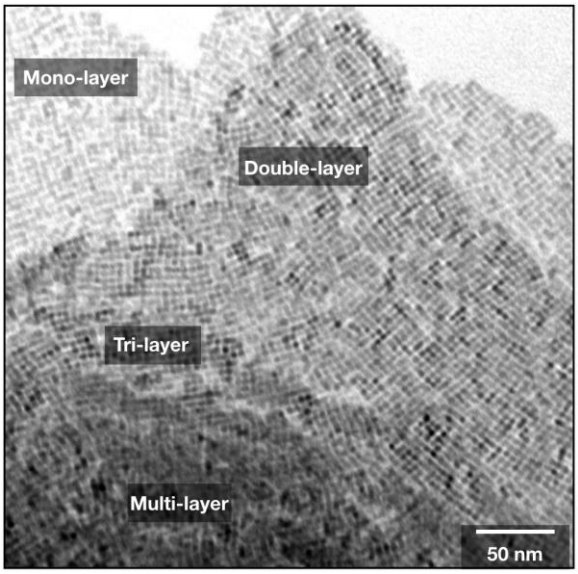

Fig. S10 The TEM image of a PbS NC film prepared by the usage of DMSO as the bottom liquid. The film shows that several domains with various numbers of NC layers (monolayer, bilayer, tri-layer, and some of the multi-layers) exhibit square lattice.

It is the reason why we limit the studies in this manuscript for NC film assemblies consisting of mostly a monolayer of NC superlattice, especially for the transport measurements. Obviously, in the monolayer films, there are still some small cracks/voids or the "domain boundaries", but not significant in numbers. Thus, they would not influence the charge transport so much. For the direct evidence, there are no large cracks/voids from the TEM images in Figure S5 in the micrometre scale. Furthermore, since it is an equilibrium process, liquid/air assembly technique is known for giving fewer cracks and voids than the other NC assembly methods. As we used EDLTs for the transport measurements, if there are significantly large cracks/voids, the device will show large leak current, since the film is mostly monolayer. Once the device is working as intended, it suggests that there are no large cracks/voids generated that affect the charge transport. The relatively narrow distribution of electron mobility values extracted from these devices indicates that the electronic properties of the monolayers are similar to each other. This convergence would also suggest that the degree of any remaining cracks and voids are the same.

Reference

1 R. C. Keitel, M. C. Weidman and W. A. Tisdale, *J. Phys. Chem. C*, 2016, **120**, 20341–20349.
2 W. Xie and C. D. Frisbie, *J. Phys. Chem. C*, 2011, **115**, 14360–14368.
3 Y. Xia, J. Cho, B. Paulsen, C. D. Frisbie and M. J. Renn, *Appl. Phys. Lett.*, 2009, **94**, 013304.
4 H. Yuan, H. Shimotani, J. Ye, S. Yoon, H. Aliah, A. Tsukazaki, M. Kawasaki and Y. Iwasa, *J. Am. Chem. Soc.*, 2010, **132**, 18402–18407.
5 K. Whitham, J. Yang, B. H. Savitzky, L. F. Kourkoutis, F. Wise and T. Hanrath, *Nat. Mater.*, 2016, **15**, 557–563.

6 S. Z. Bisri, C. Piliego, M. Yarema, W. Heiss and M. A. Loi, *Adv. Mater.*, 2013, **25**, 4309–4314.
7 M. I. Nugraha, R. Häusermann, S. Z. Bisri, H. Matsui, M. Sytnyk, W. Heiss, J. Takeya and M. A. Loi, *Adv. Mater.*, 2015, **27**, 2107–2112.
8 A. G. Shulga, L. Piveteau, S. Z. Bisri, M. V. Kovalenko and M. A. Loi, *Adv. Electron. Mater.*, 2016, **2**, 1500467.
9 M. Zhao, F. Yang, C. Liang, D. Wang, D. Ding, J. Lv, J. Zhang, W. Hu, C. Lu and Z. Tang, *Adv. Funct. Mater.*, 2016, **26**, 5182–5188.
10 W. Koh, S. R. Saudari, A. T. Fafarman, C. R. Kagan and C. B. Murray, *Nano Lett.*, 2011, **11**, 4764–4767.
11 M. Alimoradi Jazi, V. A. E. C. Janssen, W. H. Evers, A. Tadjine, C. Delerue, L. D. A. Siebbeles, H. S. J. van der Zant, A. J. Houtepen and D. Vanmaekelbergh, *Nano Lett.*, 2017, **17**, 5238–5243.
12 D. V. Talapin, *Science.*, 2005, **310**, 86–89.
13 Q. Lin, H. J. Yun, W. Liu, H.-J. Song, N. S. Makarov, O. Isaienko, T. Nakotte, G. Chen, H. Luo, V. I. Klimov and J. M. Pietryga, *J. Am. Chem. Soc.*, 2017, **139**, 6644–6653.
14 Y. Liu, J. Tolentino, M. Gibbs, R. Ihly, C. L. Perkins, Y. Liu, N. Crawford, J. C. Hemminger and M. Law, *Nano Lett.*, 2013, **13**, 1578–1587.